nature communications

Article

https://doi.org/10.1038/s41467-024-54938-z

Neurotransmitter-bound bestrophin channel structures reveal small molecule drug targeting sites for disease treatment

Received: 18 December 2023

Accepted: 15 November 2024

Published online: 30 December 2024

Check for updates

Aaron P. Owji[1,2], Jingyun Dong[1,2], Alec Kittredge[1], Jiali Wang[1], Yu Zhang[1] ✉ & Tingting Yang[1] ✉

Best1 and Best2 are two members of the bestrophin family of anion channels critically involved in the prevention of retinal degeneration and maintenance of intraocular pressure, respectively. Here, we solved glutamate- and γ-aminobutyric acid (GABA)-bound Best2 structures, which delineate an intracellular glutamate binding site and an extracellular GABA binding site on Best2, respectively, identified extracellular GABA as a permeable activator of Best2, and elucidated the co-regulation of Best2 by glutamate, GABA and glutamine synthetase in vivo. We further identified multiple small molecules as activators of the bestrophin channels. Extensive analyses were carried out for a potent activator, 4-aminobenzoic acid (PABA): PABA-bound Best1 and Best2 structures are solved and illustrate the same binding site as in GABA-bound Best2; PABA treatment rescues the functional deficiency of patient-derived Best1 mutations. Together, our results demonstrate the mechanism and potential of multiple small molecule candidates as clinically applicable drugs for bestrophin-associated diseases/conditions.

The bestrophins, with four members in mammals, are a family of Ca^{2+}-activated anion channels widely distributed across various human organs such as the airways, colon, kidney, pancreas and central nervous system[1]. They are especially important for their physiological roles in the eye[1]. Notably, Best1 is primarily expressed in the retinal pigment epithelium (RPE) and is genetically linked to a range of retinal degenerative diseases collectively referred to as bestrophinopathies[2,3], which can be clinically diagnosed by any of over 350 different Best1 mutations, mostly resulting in a loss-of-function (LOF) phenotype[1,2]. These conditions cause progressive vision loss in patients, often leading to blindness, and currently lack effective treatment[4]. Meanwhile, Best2 is found in the non-pigmented epithelium (NPE) and plays an essential role in regulating intra-ocular pressure (IOP), a critical factor for eye health, as both ocular hypertension and hypotension are deleterious[5–7]. Therefore, bestrophins are considered promising drug targets, particularly for eye disorders.

However, this request is prohibited by the poor knowledge of small molecule activators or inhibitors specific for the bestrophin channels. Ca^{2+} was first identified as an essential activator of bestrophins, leading to the classification of this protein family as Ca^{2+}-activated anion channels[8,9]. Later on, ATP was found to be required for the activation of a bacterial bestrophin homolog which lacks the Ca^{2+}-binding site and for the full activation of mammalian bestrophins in the presence of Ca^{2+}[10]. As Ca^{2+} and ATP are both common physiological molecules involved in numerous biochemical activities, neither of them or their analogs is suited for pharmaceutically targeting bestrophins.

Besides Ca^{2+} and ATP, we recently reported that intracellular glutamate is permeable for Best2, strongly promotes Best2 channel function and relieves the inhibitory effect of glutamine synthetase (GS), which binds to Best2 on the intracellular side[11]. However, extracellular glutamate is barely permeable for Best2 and does not have these promotive effects[11], suggesting the binding of glutamate to Best2

[1]Department of Ophthalmology, Columbia University, New York, NY, USA. [2]These authors contributed equally: Aaron P. Owji, Jingyun Dong.
✉e-mail: yz3802@cumc.columbia.edu; ty2190@cumc.columbia.edu

on the intracellular side, which represents a delivery problem for the potential usage of glutamate analogs as bestrophin activators in vivo. Interestingly, Best1 has been shown to be permeable to both glutamate and γ-aminobutyric acid (GABA), the major excitatory and inhibitory neurotransmitter, respectively, when natively expressed in astrocytes and heterologously co-expressed with glutamic acid decarboxylase 65 (GAD65) in HEK293 cells[12–16], but the permeability and influence of GABA on Best2 are still unknown.

Previous studies have revealed several key structural components on the pentameric assembly of bestrophins for controlling the channel function. These include: (1) two major permeation constrictions in the ion conducting pathway, namely the "neck" (I76/F80/F84 in Best1 and Best2) at the transmembrane pore and the "aperture" (I205/Q208/N212 in Best1 and S205/K208/E212 in Best2) at the cytosolic exit[17–21]; (2) a C-terminal autoinhibitory segment (AS, residues 346-378/379 in Best1/Best2), which constricts the channel concentrically by wrapping around the channel periphery in an inter-protomer manner, and unleashes in concomitant with neck opening[21–23]; (3) a Ca^{2+}-clasp formed by an acidic cluster between S4a and S4b (E300/D301/D302/D303/D304 in Best1/Best2) from one protomer and the N-terminal S1a-S1b helix-turn-helix element of an adjacent protomer[17,21]. One would expect that small molecule activators/inhibitors, such as glutamate and ATP, affect the conformation of one or more of these components, but the specific mechanisms remain unclear due to the lack of activator/inhibitor-bound bestrophin co-structures.

In this work, we identify multiple small molecules as bestrophin activators including glutamate, γ-aminobutyric acid (GABA) and 4-aminobenzoic acid (PABA), and show the co-structures of Best2-glutamate, Best2-GABA, Best1-PABA and Best2-PABA, which illustrate an intracellular glutamate binding site and an extracellular GABA/PABA binding site, revealing two distinct allosteric mechanisms. Importantly, PABA treatment rescues the functional deficiency of patient-derived Best1 mutations, underlying a potential treatment strategy for bestrophin-associated diseases/conditions.

Results

Glutamate-bound Best2 structure

We recently reported that glutamate promotes Best2 function specifically from the intracellular/cytosolic side of the channel with a half maximal effective concentration (EC_{50}) at 46 mM[11]. To test if glutamate has a similar effect on Best1, both paralogs were individually transfected into HEK293 cells, followed by whole-cell patch clamp recordings. Consistent with our previous results, outward currents (Cl^- influx) from cells expressing Best2 were significantly increased with glutamate replacing Cl^- as the principal anion in the internal solution (Supplementary Fig. 1a). By sharp contrast, outward (Cl^-) currents from cells expressing Best1 were not affected by intracellular glutamate under the same conditions (Supplementary Fig. 1b), suggesting that glutamate-mediated promotion is specific to Best2, but not Best1.

To elucidate the structural basis of this stimulating effect of intracellular glutamate, we incubated purified Best2 with 50 mM glutamate prior to cryo-EM grids preparation, and solved the glutamate-bound and -unbound Best2 structures under this condition at 3.0–3.2 Å (Fig. 1a–f, Supplementary Fig. 2 and Supplementary Table 1).

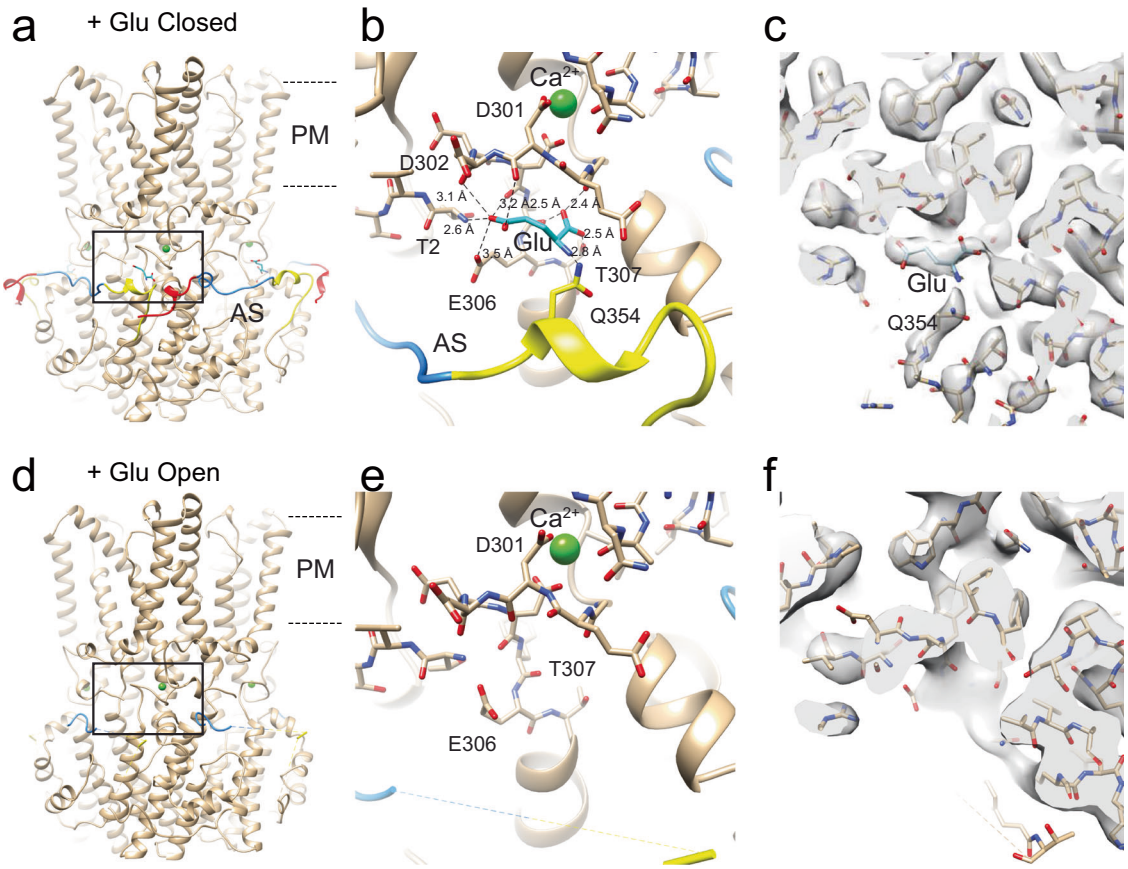

Fig. 1 | Glutamate-bound and -unbound Best2 structures. a Side view of glutamate-bound Best2 in the closed state with glutamate molecule shown as blue sticks and Ca^{2+} as a green sphere. Regions of the AS are colored as follows: ACR1, yellow; Anchor, blue; ACR2, red. PM, plasma membrane. Black box indicates region of focus in panel (**b**). **b** Close-up of the glutamate binding site with hydrogen bonds depicted as dotted lines and interacting residue side chains labeled. **c** The model and map (shown at sigma 6) of the glutamate binding site with Q354 and the bound glutamate labeled. **d**–**f** The same format as **a**–**c**, respectively, for glutamate-unbound Best2 in the fully open state from the same data set.

Consistent with the functional results, the Best2 + glutamate data set shows a significantly higher percentage of particles with a fully open neck compared to that in the glutamate-free data set from our previous study (33% vs 12%, Supplementary Fig. 2d)[11,21]. Glutamate binds to Best2 in a hydrophilic pocket just below the Ca^{2+}-clasp, making hydrogen bonds with the backbone of the Ca^{2+}-clasp, the N-terminal segment, and the C-terminal AS, all of which are critical for channel gating[21]: (1) the side chain carboxyl group of the glutamate molecule makes hydrogen bonds with the N-terminus of the N-terminal segment, the side chain carboxyl of E306, and the backbone carbonyls of D301, D302 and D304; (2) the carboxyl group of the main chain makes hydrogen bonds with the backbone carbonyls of F305, G299, and the side chain hydroxyl group of T307; (3) the amino group makes a hydrogen bond with the side chain of Q354 within the AS (Fig. 1b). Notably, due to an insertion of F353 in Best2, Q354 of Best2 showed an inward position compared to its counterpart Q353 of Best1, which may underlie the different effects of glutamate on Best1 and Best2 (Supplementary Fig. 1d, e).

Interestingly, the densities representing the glutamate molecule and the AS region, including both AS Cooperativity Regions (ACR1 and ACR2, corresponding to residues 346–356, which contains the critical residue Q354, and 369–379, respectively. Supplementary Fig. 1d), are simultaneously abolished in the open state structure (Fig. 1a–f), suggesting dissociation of the AS from the channel upon glutamate binding. As unleashing AS is required for opening the neck[21], these results indicate that: (1) glutamate binds to the closed channel and comes off upon channel opening; (2) Q354 is critical for glutamate binding. We speculate that the binding of glutamate to Best2 may sterically occlude AS from association with the channel core, thus unleashing the restriction of the neck gate[21]. Consistent with this model, intracellular glutamate could not promote currents from cells expressing a chimeric construct $Best2_{1–345}$-$Best1_{346–405}$, which contains the core region of Best2 and the AS of Best1 (Supplementary Fig. 1c).

GABA-bound Best2 structure

Glutamate and GABA are the major excitatory and inhibitory neurotransmitters, respectively. We recently discovered that GABA directly binds to Best1 and promotes opening of the neck[16]. To test if GABA has any effect on the conformation of Best2, we incubated purified Best2 proteins with GABA prior to cryo-EM grids preparation, and found that GABA binds to Best2 as well. The GABA-bound Best2 structure was solved at 2.3 Å resolution (Fig. 2a, b, Supplementary Figs. 3–5 and

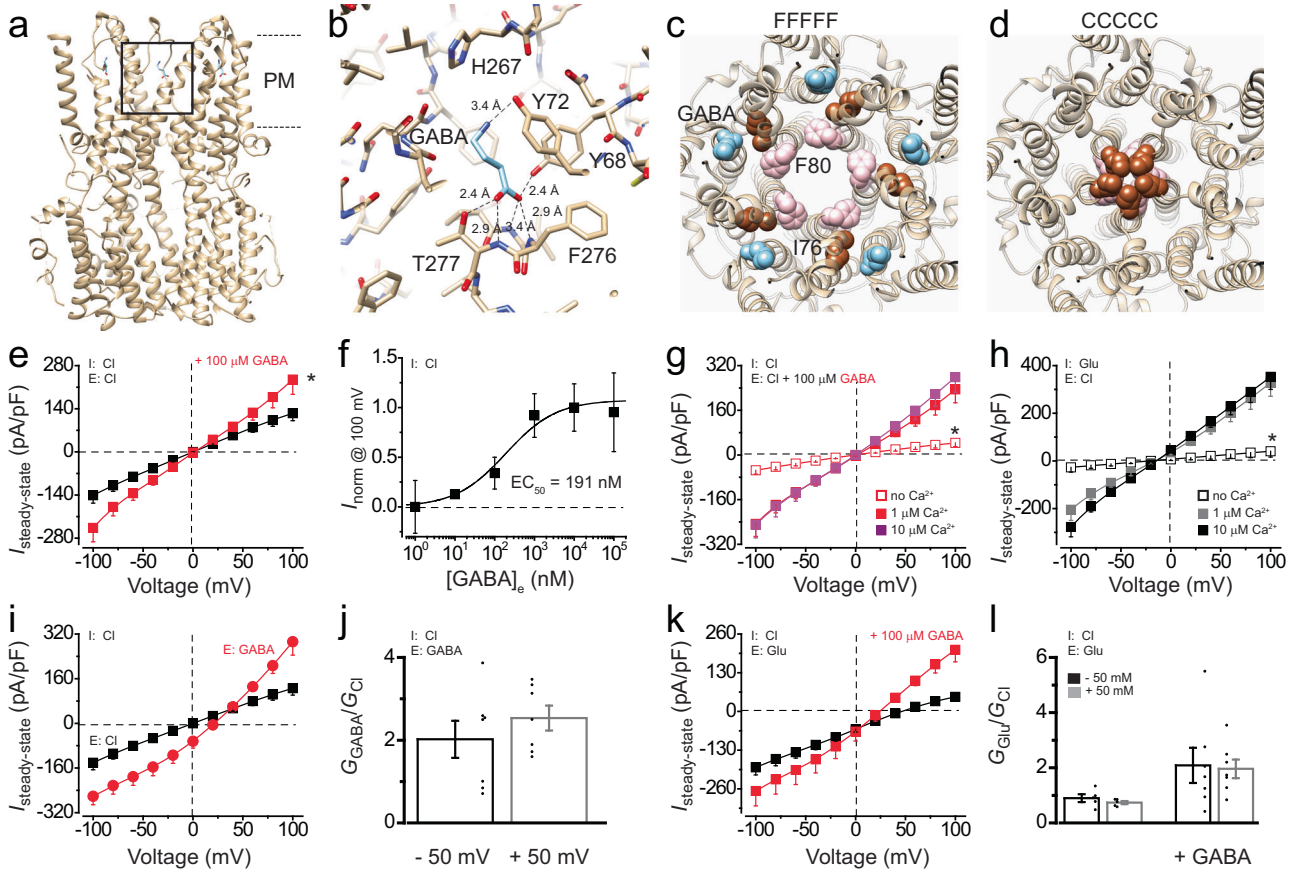

Fig. 2 | Influence of GABA on Best2 structure and function. a Side view of GABA-bound Best2 with GABA molecule shown as blue sticks. PM, plasma membrane. Black box indicates region of focus in panel (**b**). **b** Close-up of the GABA binding site with hydrogen bonds depicted as dotted lines and interacting residue side chains labeled. **c, d** Top views of Best2 (from the extracellular side) with GABA molecules shown as blue spheres, I76 as brown spheres, and F80/F84 as pink spheres in the fully open (FFFFF, **c**) and closed (CCCCC, **d**) states. **e** Population steady-state current density-voltage (I-V) relationships of Best2 in HEK293 cells at 1 μM $[Ca^{2+}]_i$ when Cl^- is the principal anion, with or without 100 μM external GABA; n = 6–9 for each point; $^*p < 0.05$ compared to no GABA. I, intracellular; E, extracellular. **f** Normalized steady-state current density at +100 mV (Y axis) plotted against different concentrations of external GABA (X axis) and fitted to the Hill equation; n = 6–9 for each point. **g, h** I-V relationships of Best2 in HEK293 cells, with Cl^- as the principal anion and 100 μM GABA in the external solution (**g**), or with internal glutamate and external Cl^- (**h**); n = 5–7 for each point, $^*p < 0.05$ compared to 1 μM $[Ca^{2+}]_i$. **i** I-V relationships of Best2 at 1 μM $[Ca^{2+}]_i$ when Cl^- is the principal anion (black), compared to that when GABA is the principal ion in the external solution; n = 7–9 for each point. **j** Relative ion conductance ratios (G_{GABA}/G_{Cl}) measured as slope conductance at the reversal potential plus 50 mV (GABA/Cl, gray) or minus 50 mV (Cl/Cl, black) at 1 μM $[Ca^{2+}]_i$; n = 7 for each bar. **k** I-V relationships of Best2 at 1 μM $[Ca^{2+}]_i$ with internal Cl^- and external glutamate, in the absence or presence of 100 μM external GABA; n = 5–7 for each point. **l** G_{Glu}/G_{Cl} in the absence or presence of 100 μM GABA; n = 5–7 for each bar. *P* values are calculated using two-tailed unpaired Student's *t* test. All error bars in this figure represent s.e.m.

Supplementary Table 1), illustrating an extracellular GABA binding site resembling that in Best1 and previously identified as a Cl^- binding site by X-ray anomalous diffraction with chicken Best1[16,17]. There are six hydrogen bonds formed between GABA and Best2 (Fig. 2b): an oxygen atom in the GABA carboxyl group forms three hydrogen bonds, one with the side chain hydroxyl of Y68 (2.4 Å) and two with the backbone nitrogen atoms of I275 (3.4 Å) and F276 (2.9 Å); the other oxygen atom in the GABA carboxyl group forms two hydrogen bonds, one with the backbone nitrogen atom of T277 (2.9 Å) and the other with the side chain hydroxyl group of T277 (2.4 Å); the nitrogen atom in the GABA amino group forms a hydrogen bond (3.4 Å) with the oxygen atom of the Y72 sidechain hydroxyl group.

Strikingly, 65% of particles in the Best2 + GABA data set are GABA-bound (one GABA molecule to each Best2 protomer thus five per pentamer) and display a fully open neck (Fig. 2c and Supplementary Fig. 3d), which is significantly higher compared to 33% of particles in this conformation in the Best2 + glutamate data set (Supplementary Fig. 2d), or 12% of particles in the previous data set with neither GABA nor glutamate[21]. By contrast, the remaining 35% of particles are not bound with GABA and exhibit a fully closed neck (Fig. 2d and Supplementary Fig. 3g). Taken together, our results indicate that the binding of GABA to the extracellular pocket on Best2 strongly promotes opening of the neck, resulting in the side-chains of I76/F80/F84 turning away from the channel pore (Supplementary Fig. 5a). The aperture of glutamate- or GABA-bound Best2 is indistinguishable from that of GABA-free Best2 (Supplementary Fig. 4a–d), suggesting that the binding of glutamate or GABA to Best2 does not affect the structural conformation of the aperture.

Notably, GABA binding induces a conformational change in the pore-lining helix by recruitment of Y68 to form a hydrogen bond with the GABA carboxyl group, resulting in a 1.2 Å and 1.4 Å shift of the Y72 and Y68 alpha carbons, respectively, upwards and slightly away from the central axis (Supplementary Fig. 5a). Multiple hydrogen bonds between the GABA carboxyl group and the electronegative N-terminal helix dipole anchor the GABA molecule in this pocket, while another hydrogen bond anchors Y68 in the open position and sterically occludes Y68 from undergoing the open-to-close conformational transition (Fig. 2b and Supplementary Fig. 5a, b). We hypothesize that these interactions anchor the pore-lining helix in a slightly dilated position, which, with symmetric five-fold occupancy, energetically favors unwinding of the helix at P77, leading to full opening of the neck gate.

GABA is a Best2 activator and promotes the influx of extracellular glutamate

Then, we examined how GABA affects Best2 channel function by adding GABA to the standard Cl^- patch solutions during patch clamp recordings. In alignment with the structural findings, both inward and outward Cl^- currents from Best2 transiently expressed in HEK293 cells were significantly elevated upon addition of 100 μM GABA in the external solution (Fig. 2e). To assess GABA's dose dependency, we carried out patch clamp experiments with varying GABA concentrations in the external solution. Plotting the outward current density (Cl^- influx) against extracellular GABA concentrations and fitting to the Hill equation, we determined the EC_{50} of extracellular GABA for activating Best2 as 191 nM (Fig. 2f). Markedly, both GABA and glutamate promote Best2 in a Ca^{2+}-dependent manner, and peak currents were reached at 1 μM free intracellular Ca^{2+} ($[Ca^{2+}]_i$) (Fig. 2g, h).

To test if Best2 is permeable to GABA, we used GABA as the principal passing ion in the external solution and Cl^- as the only anion in the internal solution. The reversal potential was shifted to the right (E_{rev} = 16.6 ± 5.3 mV, Fig. 2i), corresponding to a GABA to Cl^- relative permeability (P_{GABA}/P_{Cl}) of 0.56 in Best2. Moreover, substituting Cl^- in the external solution with GABA resulted in a strong increase of not only outward current (GABA influx) but also inward current (Cl^- efflux) (Fig. 2i, j). These results indicate that: (1) Best2 is permeable to extracellular GABA; (2) GABA on the extracellular side of the channel promotes Cl^- outward movement from the intracellular side in *trans*, consistent with the structural results.

Previously, we found that with external glutamate and internal Cl^-, the reversal potential of Best2 shifted significantly to the right (E_{rev} = 46.2 ± 2.5 mV, Fig. 2k, black), and permeability ratio of glutamate in relative to Cl^- (P_{Glu}/P_{Cl}) was only 0.1[11]. To test if GABA affects glutamate permeability, 100 μM GABA was added in the glutamate external solution. Under this condition, the reversal potential was significantly shifted towards the left (E_{rev} = 18.0 ± 5.5 mV, Fig. 2k, red) and the (P_{Glu}/P_{Cl}) was elevated to 0.53. Moreover, the outward glutamate and inward Cl^- currents from Best2 were both significantly increased upon the addition of 100 μM GABA in the external solution (Fig. 2k, l).

Taken together, our results show that GABA binds to Best2 on the extracellular side, promotes Best2-mediated Cl^- current at the level of nanomolar concentrations, and significantly increases the permeability of extracellular glutamate.

GABA releases GS-mediated inhibition on Best2 in vivo

Previously, we found that GS binds to Best2 and inhibits the channel function in the absence of intracellular glutamate in NPE[11]. To test if extracellular GABA relieves the inhibitory effect of GS, we examined the influence of GABA on the currents from HEK293 cells co-expressing Best2 and GS. Consistent with previous studies, when Cl^- was the only anion in the internal solution, GS significantly decreased the currents regardless of whether Cl^- or glutamate was the principal anion in the external solution (Fig. 3a, b, black). By contrast, when 100 μM GABA was added to the external solution, both Cl^- and glutamate currents were significantly increased to similar levels as those in the absence of GS (Fig. 3a, b, red), and the reversal potential under the external glutamate and internal Cl^- condition was also shifted to a similar position to that in the absence of GS (E_{rev} = 16.8 ± 4.6 mV, Fig. 3b, red) with a P_{Glu}/P_{Cl} of 0.54.

Then we examined the influence of GABA on native Best2-mediated currents in NPE cells by patch clamp under the same conditions. The results resembled those from transiently transfected HEK293 cells (Fig. 3c, d), strongly suggesting a physiological role of GABA in promoting Best2-mediated Cl^- currents and glutamate influx in NPE cells, despite the presence of GS[11].

Small molecule activators of Best1/Best2

As GABA acts as a potent activator of Best2 and its binding site is extracellular, our findings suggest the potential of small molecules to stimulate the channel function via this binding site for clinical applications. To test this idea, we employed a candidate approach with four compounds, including a GABA analog- isoguvacine, and three benzoic acid derivatives with different chemical groups at the *para* position, namely 4-aminobenzoic acid (PABA), 4-nitrobenzoic acid (PNBA) and 4-hydroxybenzoic acid (PHBA). Best2-mediated Cl^- currents were significantly elevated by 100 μM of each substance in the external solution during patch clamp recording (Fig. 4a–d and Supplementary Fig. 6a), suggesting that all four small molecules are activators of Best2.

As the residues forming the GABA-binding site on Best2 are highly conserved among bestrophins[16], we reasoned that the small molecule activators may also stimulate Best1. Indeed, Best1-mediated Cl^- currents in transiently transfected HEK293 cells were significantly enhanced by 100 μM of each small molecule in the external solution (Fig. 4e–h and Supplementary Fig. 6b).

To further investigate the dose dependency of the small molecule activators on Best1, whose loss-of-function leads to macular degeneration, we performed patch clamp analysis with a range of concentrations of PABA, PNBA, isoguvacine and PHBA in the external solution. The plots of outward current density (Cl^- influx) against extracellular small molecule concentration were fitted to the Hill

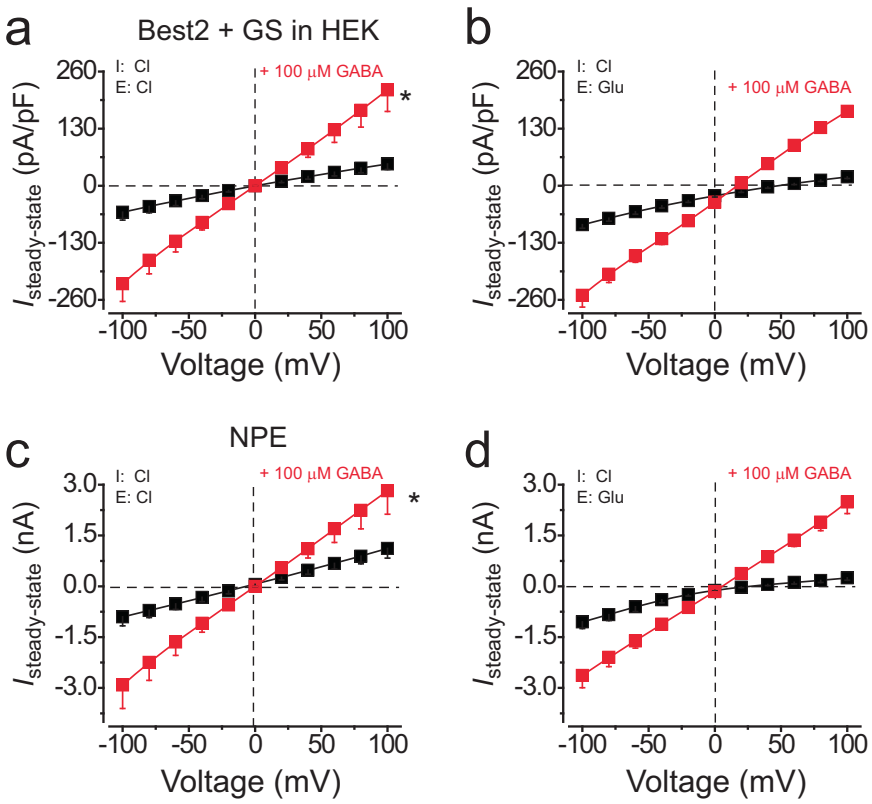

Fig. 3 | Influence of GABA on Best2 function in the presence of GS. a, **b** The I-V relationships of Best2 co-expressed with GS in HEK293 cells at 1 μM $[Ca^{2+}]_i$ in the absence (black) or presence (red) of 100 μM external GABA, when Cl^- is the principal anion in both internal and external solutions (**a**) or glutamate is the principal anion in the external solution (**b**); n = 6–8 for each point; *$p < 0.05$ compared to no GABA, using two-tailed unpaired Student's *t* test. **c**, **d** The same format as **a**, **b**, respectively, for the endogenous currents from human NPE cells; n = 5–6 for each point. All error bars in this figure represent s.e.m.

equation. The EC_{50} values required for activating Best1 were measured as 192 nM for PABA, 261 nM for PNBA, 258 nM for isoguvacine and 180 nM for PHBA (Supplementary Fig. 6c). Moreover, tiny currents were recorded in the absence of Ca^{2+} for both Best1 and Best2 with 100 μM PABA (Fig. 4a, e), indicating that the PABA-mediated activation is Ca^{2+} dependent.

PABA-bound Best1 and Best2 structures

To validate the role of the GABA-binding site in accommodating other small molecule activators of the bestrophin channels, we solved the PABA-bound Best1 and Best2 structures at 2.4–2.7 Å resolution (Fig. 5, Supplementary Figs. 7–9 and Supplementary Table 2). The PABA-bound co-structures show that PABA binds to both channels at the same site where GABA binds to Best2, retaining all the contact points seen in the GABA-Best2 co-structure, plus a hydrogen bond with H267 (Figs. 2a, b and 5, and Supplementary Fig. 5b–d). Moreover, the aromatic ring of PABA makes pi stacking and edge-to-face interactions with the side chains of F257 and Y72, respectively (Fig. 5b, f, and Supplementary Fig. 5c, d).

In the Best2 + PABA data set, a fully open neck is displayed in 57% of particles (Fig. 5c and Supplementary Fig. 7d), and a closed neck is present in 43% of particles (Fig. 5d and Supplementary Fig. 7g). In the Best1 + PABA data set, a fully open neck is displayed in 18% of particles (Fig. 5g and Supplementary Fig. 8d), while the fully closed state is completely absent and a previously unknown intermediate state consisting of two closed and three partially open protomers (PPCPC) is identified (Fig. 5h and Supplementary Figs. 8g and 9). For comparison, the majority of Best1 particles (89%) from the PABA-free condition are in the fully closed state, while the fully open neck is completely absent[21]. Taken together, our results indicate that similar to GABA, PABA binds to the extracellular side of bestrophins and strongly promotes bestrophin neck opening.

PABA rescues Best1 patient-derived mutations in HEK293 cells

As the majority of disease-causing Best1 mutations are autosomal dominant LOF mutations, the co-existence of the WT and LOF mutant Best1 proteins in patients underlies a potential therapeutic strategy for bestrophinopathies by small molecule activators of Best1[4]. To test this idea, we individually co-transfected six patient-derived dominant LOF mutants (A10T, R218H, L234P, A243T, Q293K and D302A) along with WT Best1 into HEK293 cells at a 4:1 ratio to mimic the endogenous allelic expression ratio in patient RPE cells[24–27], and examined the influence of PABA on Ca^{2+}-dependent Cl^- currents in these cells by patch clamp. Consistent with our previous results[27], all six mutations caused a decrease of Best1-mediated currents, and were fully rescued by PABA at different concentrations (Fig. 6a–f). Notably, A243T exhibits the least deficiency among the six mutants and requires the lowest concentration of PABA (10 nM) for its functional rescue, as the other mutants A10T, R218H, L234P, Q293K and D302A require 100 nM, 10 μM, 10 μM, 1 μM and 1 μM PABA, respectively. These results demonstrate the potential of PABA as a drug to treat bestrophinopathies caused by Best1 dominant LOF mutations.

Discussion

Here, we identified the inhibitory neurotransmitter GABA as an activator of Best2, defined a conserved extracellular GABA-binding site from the co-structure, and discovered several other small molecule bestrophin activators, including PABA, PNBA, PHBA and isoguvacine. Moreover, we solved the PABA-bound Best1 and Best2 structures,

https://doi.org/10.1038/s41467-024-54938-z

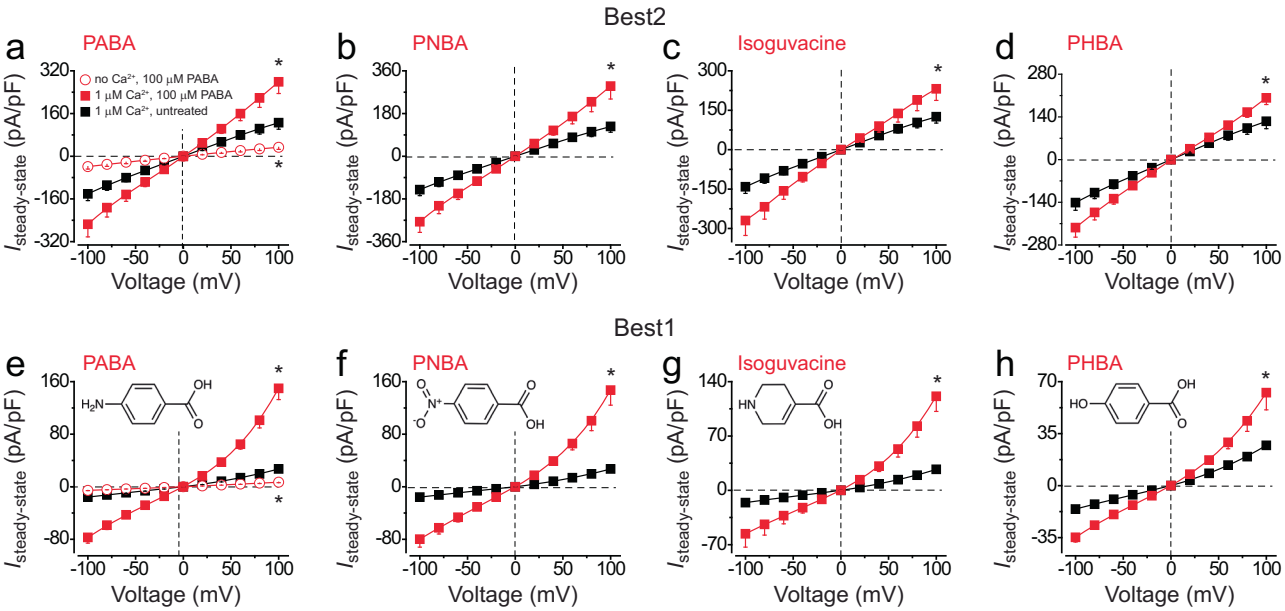

Fig. 4 | Functional influences of small compounds on bestrophin channels. **a**–**d** The I-V relationships of Best2 in transiently transfected HEK293 cells at 1 μM $[Ca^{2+}]_i$ when the principal anion is Cl^- in both internal and external solutions, without (black) or with (red solid) the treatment of 100 μM PABA (**a**), PNBA (**b**), isoguvacine (**c**), or PHBA (**d**); $n = 5–9$ for each point; *$p < 0.05$ compared to untreated cells (black), using two-tailed unpaired Student's t test. **e**–**h** The same format as **a**–**d**, respectively, for Best1; n = 6–7 for each point. The chemical structure of each compound is shown in the respective panel in **e**–**h**. All error bars in this figure represent s.e.m.

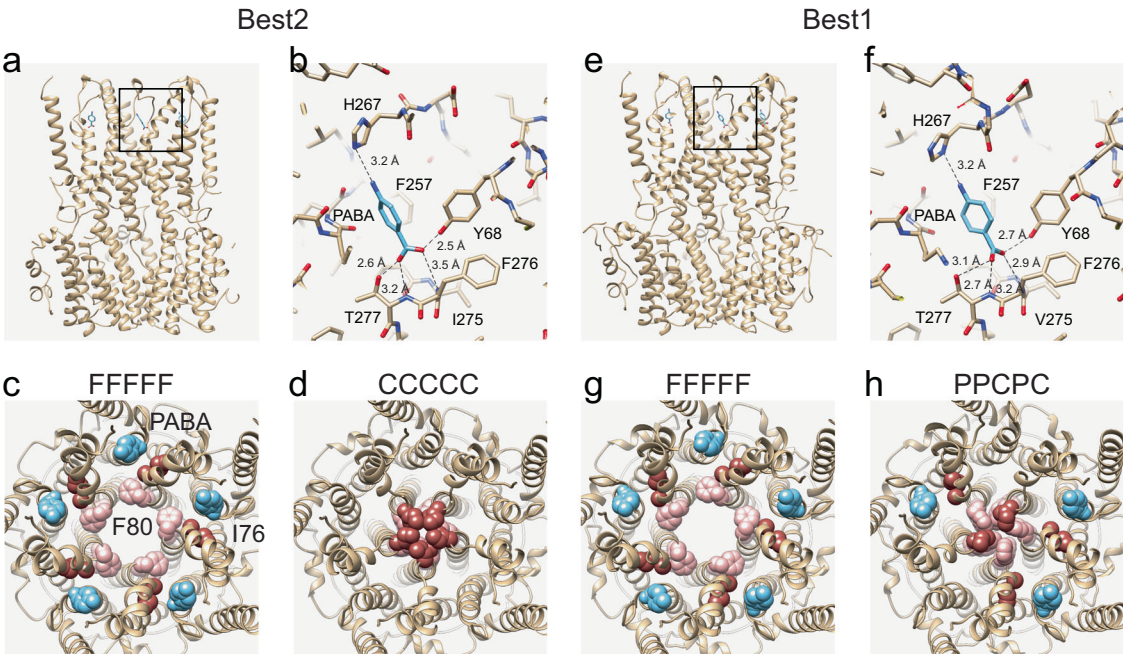

Fig. 5 | PABA-bound Best2 and Best1 structures. **a** Side view of PABA-bound Best2 with PABA molecule shown as blue sticks. Black box indicates region of focus in panel (**b**). **b** Close-up of the PABA binding site with hydrogen bonds depicted as dotted lines and interacting residue side chains labeled. **c**, **d** Top views of Best2 (from the extracellular side of the membrane) with PABA molecules shown as blue spheres, I76 as brown spheres, and F80/F84 as pink spheres in the fully open (**c**) and closed (**d**) states. **e**–**h** PABA-bound Best1 structures in the same format as **a**–**d**, respectively, except for (**h**) showing an intermediate state.

which illustrate the same binding site as that in GABA-bound Best2, and showed that PABA treatment rescues the functional deficiency of patient-derived Best1 mutations in transiently transfected HEK293 cells. Together, our results demonstrate the mechanisms of neurotransmitter-mediated activation of bestrophin channels and the potential of multiple candidate compounds as clinically applicable drugs for bestrophin-associated diseases.

We previously reported an inhibitory effect of GS on Best2 that can be alleviated by intracellular glutamate[11]. Our results from this study suggest that the GS-mediated inhibition can also be overcome by extracellular GABA. GABA also significantly enhances the permeability of Best2 to extracellular glutamate, which would further stimulate Best2 once it becomes intracellular. We speculate that this positive feedback reflects the co-regulation of Best2 by glutamate, GABA and

https://doi.org/10.1038/s41467-024-54938-z

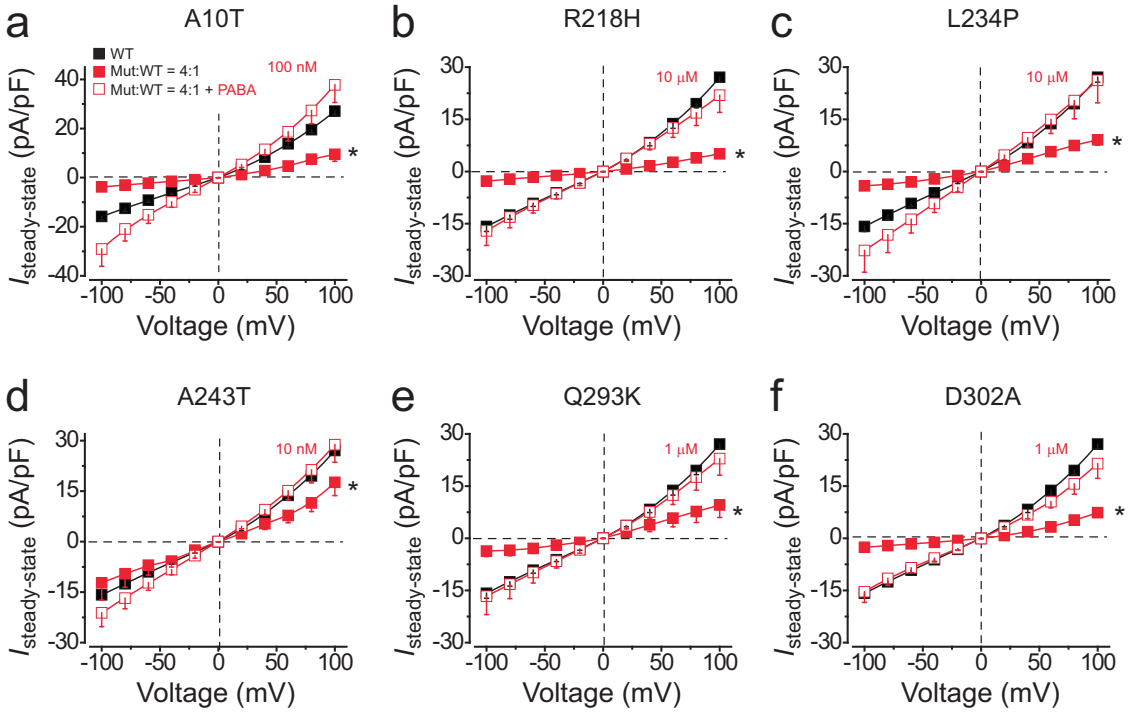

Fig. 6 | Functional rescue of Best1 patient-derived mutations by PABA. a–f The I-V relationships at 1 μM $[Ca^{2+}]_i$ in HEK293 cells transiently expressing WT Best1 alone (black, untreated), or co-expressing WT Best1 and patient-derived A10T (**a**), R218H (**b**), L234P (**c**), A243T (**d**), Q293K (**e**) and D302A (**f**) mutants at a 1:4 ratio (red) without (solid) or with (open) the treatment of PABA; n = 6–8; *$p < 0.05$ compared to untreated WT cells, using two-tailed unpaired Student's t test. All error bars in this figure represent s.e.m.

GS in NPE cells. Notably, Best2 is permeable to intracellular glutamate and extracellular GABA, suggesting a potential role of Best2 in visual synaptic transmission via mediating the permeation of both excitatory and inhibitory neurotransmitters.

Retinal degenerative bestrophinopathies are caused by Best1 mutations, most of which are autosomal dominant LOF, such that the WT Best1 protein still exists in the patients' cells and can be activated upon binding of the small molecule activator to compensate for the LOF caused by the mutations. On the other hand, Best1 recessive mutations shall be individually examined for their response to each small molecule, as there is no WT Best1 protein in these cells while the mutant Best1 may or may not be bound/activated by the small molecule activator. Although the rare Best1 gain-of-function mutations are not suited for this treatment, autosomal dominant LOF counts for >95% of all bestrophinopathy cases and thus underlies the great pharmaceutical potential of small molecule Best1 activators. This provides an alternative treatment strategy, besides gene therapy, for the cure of bestrophinopathies.

Best2 knockout mice exhibited a decrease of IOP[5,6], suggesting a positive contribution of Best2 channel function to IOP. The activation of Best2 by GABA suggests that increased GABA levels in the ciliary body could be a causal factor of ocular hypertension. Notably, experimentally induced ocular hypertension has been shown to cause a decrease of GABAergic activity in the eye[28,29], suggesting a negative feedback in the GABAergic system upon elevated IOP. On the other hand, small molecule activators of Best2 could be potentially utilized for the treatment of ocular hypotony. As the hosting residues are identical between Best1 and Best2 (Supplementary Fig. 1d), the six disease-causing Best1 mutations examined in this study would cause similar channel function defects if they occur in Best2, possibly leading to altered IOP. However, such equivalent mutations in Best2 have not been reported.

In addition to the extracellular GABA binding site, we also delineated a glutamate binding site on the cytosolic side of Best2, underlining another potential hosting site for Best2-specific small molecule activators. Notably, this glutamate binding pocket is not conserved in Best1, as the bound glutamate makes contacts with residues in the conserved Ca^{2+}-clasp and the ACR1, which is substantially different between Best1 and Best2 (Supplementary Fig. 1d, e)[21]. The ACR1 segment consists of residues 346-355 in Best1 and 346–356 in Best2, with an insertion of F353 in Best2 that offsets the residue numbers by one within this region (Supplementary Fig. 1d, e)[21]. In particular, Q354 of Best2 directly interacts with glutamate, while F354 of Best1 pushes on the Ca^{2+}-clasp and transmits the association of AS on the channel core to neck closing[21]. There's also an R356 in Best1 that comes into this region and occupies the space which could potentially accommodate glutamate, while the analogous Q357 in Best2 points away from the pocket (Supplementary Fig. 1e)[21]. Moreover, intracellular glutamate only stimulates Best2, but not Best1 or the chimeric $Best2_{1-345}$-$Best1_{346-405}$ (Supplementary Fig. 1a–c), indicating a paralog-specific promotion on Best2. Interestingly, in the presence of GABA or PABA, the AS remains bound to the fully open Best1 (Supplementary Fig. 10a, b)[16], but is dissociated from the fully open Best2 (Supplementary Fig. 10c, d), suggesting that the binding of GABA/PABA overcomes the inhibitory effect of AS in Best1. This is consistent with the smaller currents and lower open probability in Best1 compared to Best2 under the same conditions.

Our structural and electrophysiological results collectively define two allosteric modulation sites on bestrophins: an extracellular GABAergic positive allosteric modulation site, which activates the channel when bound by GABA, PABA, or their analogs; and an intracellular glutamatergic positive allosteric modulation site, which unleashes the negative effect of the C-terminal AS on neck gating. As the extracellular site is highly conserved among bestrophin paralogs but the intracellular site is not, the former represents a target for general bestrophin activators while the latter is suited for development of Best2-specific activators that would not act on Best1. Future studies may focus on further optimization of these identified small

molecules to increase their specificity and potency, representing an excellent opportunity for computer-aided and structure-based drug design.

Methods

Cell lines

HEK293 and HEK293F cells were purchased from ATCC (Cat. #CRL-1573) and Thermo Fisher Scientific (Cat. #R79007), respectively. The cells used in this study were authenticated by short tandem repeat (STR) DNA profiling and tested negative for mycoplasma contamination. HEK293 cells were cultured in DMEM (Corning, Cat. #10013CV) supplemented with 100 μg/mL penicillin-streptomycin and 10% fetal bovine serum, and HEK293F cells were cultured in FreeStyle™ 293 Expression Medium (Thermo Fisher Scientific, Cat. #12338026). Human NPE cells were purchased from ScienCell Research Laboratories (Cat. #6580), cultured in Epithelial Cell Medium (EpiCM, Cat. #4101) and authenticated by morphology. No mycoplasma contamination was found by DAPI staining.

Transfection

20–24 h before transfection, cells were split into new 3.5 cm culture dishes at 50% confluency. Plasmid transfections were conducted using the PolyJet Transfection Reagent (SignaGen, Cat. #SL100688). The transfection mix was removed after 4–8 h, and cells were washed with PBS and fed with fresh media until downstream analysis or harvest.

Electrophysiology

Whole-cell patch clamp recording was conducted 48–96 h after splitting of NPE cells or transfection of HEK293 cells with an EPC10 patch clamp amplifier (HEKA Electronics) controlled by Patchmaster v2x90.5 (HEKA)[27,30]. Micropipettes were pulled and fashioned from filamented 1.5 mm thin-walled glass (WPI Instruments). Series resistance was typically 1.5–2.5 MΩ, with no electronic series resistance compensation. Experiments were conducted at room temperature (23 ± 2 °C). Liquid junction potentials were measured and corrected using HEKA built-in functions. The standard zero Ca^{2+} pipette solution contained (mM): 146 CsCl, 2 $MgCl_2$, 5 EGTA, 2 MgATP (added fresh), 10 HEPES, pH 7.3 adjusted with NMDG. Solutions with various free Ca^{2+} concentrations were made by mixing $CaCl_2$ with EGTA as calculated by the MaxChelator Program, and the free Ca^{2+} concentration was verified using a Ca^{2+} ion-selective electrode. The standard extracellular solution contained (mM): 140 NaCl, 5 KCl, 2 $CaCl_2$, 1 $MgCl_2$, 15 glucose, 10 HEPES, pH 7.4 with NMDG. In GABA/small molecule containing solutions, 100 μM, 10 μM, 1 μM, 100 nM, 10 nM or 1 nM GABA/small molecule was added in the external solution, pH 7.4 adjusted with NMDG. In GABA/glutamate external solutions, 140 mM GABA/glutamate replaced Cl^-, pH 7.4 adjusted with NMDG. In the glutamate internal solution, 146 mM Cs-glutamate replaced CsCl, pH 7.4 adjusted with NMDG. Solution osmolarity was 290 ~ 310 mOsm/L with glucose, and ~5 mOsm lower in the internal solutions than the external solutions of the same experiment. The low and high Ca^{2+} solutions in the same set of experiments were adjusted to have the exact same osmolarity. Solution changes were performed manually.

Electrophysiological data collection and analyses

Traces were acquired at a repetition interval of 4 s[28]. Currents were sampled at 25 kHz and filtered at 5 or 10 kHz. I-V curves were generated from a group of step potentials (−100 to +100 mV from a holding potential of 0 mV). Data were processed off-line in Patchmaster. Statistical analyses were performed using built-in functions in OriginPro 8.5. Relative permeability was calculated according to the Goldman–Hodgkin–Katz equation. The relative X/Cl^- (X = GABA or glutamate, with X or Cl^- in the external solution) inward movement (outward current) conductance ($G_{X\ with\ ex\text{-}X}/G_{Cl\ with\ ex\text{-}Cl}$) was measured as slope conductance at the reversal potential plus 50 mV. The *trans* effect, representing the relative Cl^- (in the internal solution) outward movement (inward current) conductance ($G_{Cl\ with\ ex\text{-}X}/G_{Cl\ with\ ex\text{-}Cl}$) was measured as slope conductance at the reversal potential minus 50 mV. The "*n*" value in patch clamp recording figure legends indicates the total number of individual cells.

Cryo-EM sample preparation

Best1 and Best2 proteins were purified in GDN[21,31]. After nickel affinity and size exclusion chromatography, the protein was concentrated to 5 mg/mL and incubated with 20 mM GABA/PABA 1 h prior to grid production for GABA-bound Best2 and PABA-bound Best1 and Best2. To introduce glutamate, the concentrated Best2 protein was buffer exchanged into 50 mM Na-glutamate, 25 mM HEPES pH 7.8 supplemented with 0.008% GDN on a sartorius 100 kDa MWCO centrifugal concentrator. Protein was concentrated to 5 mg/mL for grid production.

2.8 μL of protein was spiked with 5 mM $CaCl_2$ and immediately applied to a plasma treated UltrAuFoil R0.6/1 on a vitrobot Mark IV, incubated for 30 s at 100% humidity and 10° C, blotted for 5–7 s at force 4 and immediately plunged into liquid ethane cooled by liquid nitrogen. Grids were screened on a glacios prior to data collection.

Data collection and image processing

Data were collected by Leginon 3.5 on a Krios. For the Best2 + glutamate dataset, 6625 movies were collected with a K3 direct electron detector in counting mode at a magnification of 105,000x, corresponding to a physical pixel size of 0.825 $Å^2$ /pix at a total dose of 59 $e^-/Å^2$, fractionated over 50 frames, corresponding to a dose rate of 1.18 $e^-/Å^2$/frame with a defocus range of −1.0 ~ −2.5 microns. Movies were aligned with MotionCorr2 via Relion-3.1 and imported to cryoSPARCv4 for further processing by PatchCTF estimation, template picking, and extraction. After initial 2D classification of 3,529,672 picked particles, 189,723 particles were selected for ab initio reconstruction and local refinement using a global mask with C5 symmetry (3.1 Å). Particles underwent symmetry expansion (C5) to generate 948,615 particles, which underwent 3D classification into 3 classes using a mask encompassing the transmembrane domain. One class was in the fully open state and the other two classes were closed. The open state particles were local refined with C1 symmetry using a global mask, resulting in a final map at 3.15 Å. The 635,068 closed state particles were local refined to 3.03 Å with a global mask.

For the Best2 + GABA dataset, 1130 K3 movies were collected with a K3 direct electron detector in counting mode at a magnification of 105,000x, corresponding to a physical pixel size of 0.83 $Å^2$/pix at a total dose of 58 $e^-/Å^2$, fractionated over 50 frames, corresponding to a dose rate of 1.16 $e^-/Å^2$/frame with a defocus range of −0.8 ~ −1.5 microns. K3 movies underwent MotionCorr2 via the Relion-3.1 GUI and doseweighted micrographs were imported to cryoSPARCv4 for further processing by PatchCTF correction, template picking, extraction, and initial 2D classification resulting in 161,366 consensus particles. These particles underwent homogeneous refinement (C5) and 3D classification with a mask encompassing the neck gate and ligand binding site into 6 classes with a target resolution of 3.4 Å. 3D classification was performed without symmetry expansion. 4 classes were in the fully open neck conformation, representing 65.4% of total particles (105,576 particles), while 2 classes were fully closed. The fully open particles were refined and underwent polishing in relion. The final 103,839 particles underwent homogeneous refinement (C5) to 2.31 Å. Particles representing the closed state were similarly refined, polished in relion, and the final 54,947 polished particles underwent homogeneous refinement to 2.27 Å. 3D classification was performed and no heterogeneity within the neck was found within the separated open and closed states.

For the Best1 + PABA dataset, 1634 micrographs were collected with a K3 direct electron detector in counting mode at a magnification of 105,000x, corresponding to a physical pixel size of 0.83 $Å^2$/pix at a

total dose of 58 $e^-/Å^2$, fractionated over 50 frames, corresponding to a dose rate of 1.16 $e^-/Å^2$/frame with a defocus range of 0.8 - 1.8 microns. Movies were aligned with MotionCorr2 via Relion3.1 and imported to cryoSPARCv4 for further processing by PatchCTF estimation, template picking and extraction, and initial 2D classification resulting in 46,097 final particles. These particles underwent homogeneous refinement (C5), Bayesian polishing, symmetry expansion (generating 230,485 particles), and 3D classification with a mask encompassing the neck gate and ligand binding site into 6 classes with a target resolution of 3.2 Å. One class (41,771 particles, 18.1%) was fully open and underwent local refinement (C1) to 2.60 Å. At least three classes represent an intermediate state. All closed particles were combined and symmetry unexpanded (to remove duplicates), leaving 40,311 particles, and refined against the intermediate state volume which was obtained by reconstruction of one intermediate state from 3D classification with symmetry expansion. Homogeneous refinement with symmetry relaxation (marginalization method) was performed with a 4 Å lowpass filter to force protomer classification with high resolution features. The resulting density was nearly identical to the intermediate state obtained by reconstruction of closed symmetry expanded particles obtained from 3D classification, except the density for intermediate neck states became enhanced, likely due to suboptimal classification of the unwound helix during 3D classification. After homogeneous refinement (C5) with symmetry relaxation, particles underwent a final round of homogeneous refinement with no symmetry imposed (C1) and a lowpass filter of 4 Å to maintain the original alignments from the symmetry relaxed refinement.

For the Best2 + PABA dataset, 1053 movies were collected with a K3 direct electron detector in counting mode at a magnification of 105,000x, corresponding to a physical pixel size of 0.8215 $Å^2$/pix at a total dose of 50.52 $e^-/Å^2$, fractionated over 40 frames, corresponding to a dose rate of 1.26 $e^-/Å^2$/frame with a defocus range of -0.8 ~ -1.8 microns. K3 movies underwent motion correction by MotionCorr2 via Relion 3.1 GUI and doseweighted micrographs were imported to cryoSPARCv4 for further processing by PatchCTF correction, template picking, extraction, and initial 2D classification resulting in 47,438 final particles. These particles underwent homogeneous refinement (C5), Bayesian polishing in Relion, symmetry expansion, and a single round of focused 3D classification (5 classes, target resolution 3.4 Å) with a mask encompassing the transmembrane neck gate and the PABA binding site. 2 classes representing fully closed state were combined, symmetry unexpanded (to remove duplicates), leaving 26,692 particles, and underwent homogeneous refinement (C5) to 2.6 Å. 3 classes representing the fully open state were combined and symmetry unexpanded (remove duplicates), leaving 33,154 particles, which underwent homogeneous refinement (C5) to 2.4 Å. No intermediate state with partially open neck was identified, despite extensive 3D classification. Each final state underwent another round of focused 3D classification to ensure conformational homogeneity.

Model refinement and validation

Maps used for model building and refinement were obtained by sharpening to a b-factor determined by Guinier plot as implemented in cryoSPARC. PDB 8D1I (for Best1) and PDBs 8D1E and 8D1G (for Best2) were rigid body fit into their respective cryo-EM maps and subjected to multiple iterations of refinement in coot, phenix real space refinement, and REFMAC5 (Servalcat)[32–36]. Validation was performed with comprehensive cryo-EM validation tools in phenix, including MolProbity[37].

Statistics and reproducibility

A sufficient number of samples were examined to reach statistical conclusion according to the specific method utilized in that experiment. Statistically significant differences ($p < 0.05$) between means of two groups were determined by two-tailed unpaired Student's t test. Data are presented as means values +/− SEM.

Reporting summary

Further information on research design is available in the Nature Portfolio Reporting Summary linked to this article.

Data availability

The data that support this study are available from the corresponding authors upon request. The cryo-EM density maps have been deposited in the Electron Microscopy Data Bank (EMDB) under accession codes EMD-47304 (BEST2 + glutamate open), EMD-47305 (BEST2 + glutamate closed), EMD-47306 (BEST2 + GABA open), EMD-47307 (BEST2 + GABA closed), EMD-47308 (BEST1 + PABA open), EMD-47309 (BEST1 + PABA intermediate), EMD-47310 (BEST2 + PABA open), EMD-47311 (BEST2 + PABA closed). The atomic coordinates have been deposited in the Protein Data Bank (PDB) under accession codes 9DYH (BEST2 + glutamate open), 9DYI (BEST2 + glutamate closed), 9DYJ (BEST2 + GABA open), 9DYK (BEST2 + GABA closed), 9DYL (BEST1 + PABA open), 9DYM (BEST1 + PABA intermediate), 9DYN (BEST2 + PABA open), 9DYO (BEST2 + PABA closed). Previously published models 8D1I, 8D1G, and 8D1E are used. The source data underlying Figs. 2–4, 6 and Supplementary Figs. 1 and 6 are provided in a Source Data file. Source data are provided with this paper.

References

1. Owji, A. P., Kittredge, A., Zhang, Y. & Yang, T. Structure and Function of the Bestrophin family of calcium-activated chloride channels. *Channels (Austin)* **15**, 604–623 (2021).
2. Johnson, A. A. et al. Bestrophin 1 and retinal disease. *Prog. Retin. Eye Res.* https://doi.org/10.1016/j.preteyeres.2017.01.006 (2017).
3. Petrukhin, K. et al. Identification of the gene responsible for Best macular dystrophy. *Nat. Genet.* **19**, 241–247 (1998).
4. Yang, T., Justus, S., Li, Y. & Tsang, S. H. BEST1: the best target for gene and cell therapies. *Mol. Ther. J. Am. Soc. Gene Ther.* **23**, 1805–1809 (2015).
5. Bakall, B. et al. Bestrophin-2 is involved in the generation of intraocular pressure. *Investig. Ophthalmol. Vis. Sci.* **49**, 1563–1570 (2008).
6. Zhang, Y. et al. Enhanced inflow and outflow rates despite lower IOP in bestrophin-2-deficient mice. *Investig. Ophthalmol. Vis. Sci.* **50**, 765–770 (2009).
7. Zhang, Y., Patil, R. V. & Marmorstein, A. D. Bestrophin 2 is expressed in human non-pigmented ciliary epithelium but not retinal pigment epithelium. *Mol. Vis.* **16**, 200–206 (2010).
8. Sun, H., Tsunenari, T., Yau, K. W. & Nathans, J. The vitelliform macular dystrophy protein defines a new family of chloride channels. *Proc. Natl. Acad. Sci. USA* **99**, 4008–4013 (2002).
9. Tsunenari, T. et al. Structure-function analysis of the bestrophin family of anion channels. *J. Biol. Chem.* **278**, 41114–41125 (2003).
10. Zhang, Y. et al. ATP activates bestrophin ion channels through direct interaction. *Nat. Commun.* **9**, 3126 (2018).
11. Owji, A. P. et al. Bestrophin-2 and glutamine synthetase form a complex for glutamate release. *Nature* **611**, 180–187 (2022).
12. Lee, S. et al. Channel-mediated tonic GABA release from glia. *Science* **330**, 790–796 (2010).
13. Woo, D. H. et al. TREK-1 and Best1 channels mediate fast and slow glutamate release in astrocytes upon GPCR activation. *Cell* **151**, 25–40 (2012).
14. Jo, S. et al. GABA from reactive astrocytes impairs memory in mouse models of Alzheimer's disease. *Nat. Med.* **20**, 886–896 (2014).
15. Park, H. et al. High glutamate permeability and distal localization of Best1 channel in CA1 hippocampal astrocyte. *Mol. Brain* **6**, 54 (2013).
16. Wang, J. et al. GAD65 tunes the functions of Best1 as a GABA receptor and a neurotransmitter conducting channel. *Nat. Commun.* **15**, 8051 (2024).
17. Kane Dickson, V., Pedi, L. & Long, S. B. Structure and insights into the function of a Ca(2+)-activated Cl(-) channel. *Nature* **516**, 213–218 (2014).

18. Yang, T. et al. Structure and selectivity in bestrophin ion channels. *Science* **346**, 355–359 (2014).
19. Ji, C. et al. Dual Ca(2+)-dependent gates in human Bestrophin1 underlie disease-causing mechanisms of gain-of-function mutations. *Commun. Biol.* **2**, 240 (2019).
20. Owji, A. P. et al. Structural and functional characterization of the bestrophin-2 anion channel. *Nat. Struct. Mol. Biol.* **27**, 382–391 (2020).
21. Owji, A. P. et al. Structures and gating mechanisms of human bestrophin anion channels. *Nat. Commun.* **13**, 3836 (2022).
22. Qu, Z., Cui, Y. & Hartzell, C. A short motif in the C-terminus of mouse bestrophin 3 [corrected] inhibits its activation as a Cl channel. *FEBS Lett.* **580**, 2141–2146 (2006).
23. Qu, Z. Q., Yu, K., Cui, Y. Y., Ying, C. & Hartzell, C. Activation of bestrophin Cl- channels is regulated by C-terminal domains. *J. Biol. Chem.* **282**, 17460–17467 (2007).
24. Kittredge, A., Ji, C., Zhang, Y. & Yang, T. Differentiation, maintenance, and analysis of human retinal pigment epithelium cells: a disease-in-a-dish model for BEST1 mutations. *J. Vis. Exp.* https://doi.org/10.3791/57791 (2018).
25. Kittredge, A., Zhang, Y. & Yang, T. Evaluating BEST1 mutations in pluripotent stem cell-derived retinal pigment epithelial cells. *Methods Enzymol.* **654**, 365–382 (2021).
26. Li, Y. et al. Patient-specific mutations impair BESTROPHIN1's essential role in mediating Ca2+-dependent Cl- currents in human RPE. *eLife* **6** https://doi.org/10.7554/eLife.29914 (2017).
27. Zhao, Q. et al. Distinct expression requirements and rescue strategies for BEST1 loss- and gain-of-function mutations. *eLife* **10** https://doi.org/10.7554/eLife.67622 (2021).
28. Gramlich, O. W., Godwin, C. R., Wadkins, D., Elwood, B. W. & Kuehn, M. H. Early functional impairment in experimental glaucoma is accompanied by disruption of the GABAergic system and inceptive neuroinflammation. *Int. J. Mol. Sci.* **22** https://doi.org/10.3390/ijms22147581 (2021).
29. Moreno, M. C. et al. Effect of ocular hypertension on retinal GABAergic activity. *Neurochem. Int.* **52**, 675–682 (2008).
30. Ji, C. et al. Investigation and restoration of BEST1 activity in patient-derived RPEs with dominant mutations. *Sci. Rep.* **9**, 19026 (2019).
31. Kittredge, A., Ward, N., Hopiavuori, A., Zhang, Y. & Yang, T. Expression and purification of mammalian bestrophin ion channels. *J. Vis. Exp.* https://doi.org/10.3791/57832 (2018).
32. Afonine, P. V. et al. Real-space refinement in PHENIX for cryo-EM and crystallography. *Acta Crystallogr. D Struct. Biol.* **74**, 531–544 (2018).
33. Emsley, P. & Cowtan, K. Coot: model-building tools for molecular graphics. *Acta Crystallogr. D Biol. Crystallogr.* **60**, 2126–2132 (2004).
34. Kovalevskiy, O., Nicholls, R. A., Long, F., Carlon, A. & Murshudov, G. N. Overview of refinement procedures within REFMAC5: utilizing data from different sources. *Acta Crystallogr. D. Struct. Biol.* **74**, 215–227 (2018).
35. Murshudov, G. N. et al. REFMAC5 for the refinement of macromolecular crystal structures. *Acta Crystallogr. D. Biol. Crystallogr.* **67**, 355–367 (2011).
36. Paavo, M. et al. Mutations in GPR143/OA1 and ABCA4 inform interpretations of short-wavelength and near-infrared fundus autofluorescence. *Investig. Ophthalmol. Vis. Sci.* **59**, 2459–2469 (2018).
37. Williams, C. J. et al. MolProbity: more and better reference data for improved all-atom structure validation. *Protein Sci. Publ. Protein Soc.* **27**, 293–315 (2018).

Acknowledgements

We thank the Unrestricted Grant from Research to Prevent Blindness (RPB) to the Department of Ophthalmology at Columbia University. Cryo-EM data were collected at the Columbia Cryo-EM Core, the National Center for Cryo-EM Access and Training (NCCAT) and the Simons Electron Microscopy Center located at the New York Structural Biology Center, supported by the NIH Common Fund Transformative High Resolution Cryo-Electron Microscopy program (U24 GM129539) and by grants from the Simons Foundation (SF349247) and NY State Assembly. T.Y. was supported by NIH grants R35GM149252, R01GM127652 and R24EY028758, the Irma T. Hirschl/Monique Weill-Caulier Research Award (CU20-4313) and RPB Career Advancement Award (CU22-1892).

Author contributions

A.P.O. designed research, performed protein purification and cryo-EM experiments, analyzed data, made figures and helped write the paper; J.D. performed patch clamp recordings, analyzed data and made figures; A.K. designed research, generated constructs, performed protein purification, analyzed data and made figures; J.W. performed patch clamp recordings and analyzed data; Y.Z. and T.Y. designed research, analyzed data, made figures and wrote the paper.

Competing interests

Provisional Patents on glutamate (no. 63/693,687) and GABA/PABA (no. 63/693,686) analogs as bestrophin activators have been filed, listing A.P.O., Y.Z., and T.Y. as inventors. The remaining authors declare no competing interests.

Additional information

Supplementary information The online version contains supplementary material available at https://doi.org/10.1038/s41467-024-54938-z.

Correspondence and requests for materials should be addressed to Yu Zhang or Tingting Yang.

Peer review information *Nature Communications* thanks Lonnie P. Wollmuth and the other, anonymous, reviewer(s) for their contribution to the peer review of this work. A peer review file is available.